

# Applicability of the TESPEL Charge-Exchange Recombination Spectroscopy Diagnostics for Impurity Transport Study on LHD

KALININA Diana, SUDO Shigeru<sup>1</sup>, TAMURA Naoki<sup>1</sup>, SERGEEV Vladimir Yu.<sup>2</sup>  
and LHD Experimental group

Graduate University for Advanced Studies, Kanagawa, 240-0193, Japan

<sup>1</sup>National Institute for Fusion Science, Toki, 509-5292, Japan

<sup>2</sup>State Technical University, Politechnicheskaya 29, St. Petersburg, Russia

(Received: 9 December 2003 / Accepted: 1 April 2004)

## Abstract

Using the theoretical optimization of the Tracer Encapsulated Solid Pellet (TESPEL) Charge eXchange Recombination (CXRe) signals for various impurities in the visible spectral range under the conditions of the Large Helical Device (LHD) plasma, the TESPEL CXRe Spectroscopic (CXRS) experiments with tracer materials, such as fluorine and magnesium and impurity amounts of about  $10^{17}$ – $10^{18}$  particles have been done. For comparison with the TESPEL pellet case, the CXRe emissions from other materials after the pure impurity injection, such as neon and carbon with bigger impurity amount ( $2 \times 10^{19}$ ) were investigated. Adaptability of the TESPEL CXRS diagnostics in the ultra soft X-ray (USXR) spectral range have been discussed.

## Keywords:

TESPEL, impurity pellet, impurity transport, CXRS

## 1. Introduction

The properties of local impurity transport with fairly high-accuracy could be obtained by means of the tracer-encapsulated solid pellet (TESPEL) injection, which has been utilized previously on the Compact Helical System (CHS) and now on the Large Helical Device (LHD) [1]. TESPEL consists of polystyrene ( $-\text{CH}(\text{C}_6\text{H}_5)\text{CH}_2-$ ) as outer shell (typically 0.5–0.9 mm diameter) and tracer particles as an inner core (~0.2 mm size). The flexible choice of the tracer particle is one of the important characteristics of the TESPEL method. The behavior of impurity tracer ions deposited locally in the core plasma by means of TESPEL injection can be measured by the observation of the line emission due to the charge exchange reaction of the injected impurities. This method allows us to estimate the local impurity transport coefficients, which are already obtained by Li III on CHS. In TESPEL CXRS experiments with the LiH tracer on LHD, however, Li III ( $\lambda_{\text{Li}} = 449.9$  nm) emission in the visible spectral range could not be measured [2,3]. At a fixed magnetic geometry of the experiment, and Neutral Beam Injection (NBI) energy and power, the CXRe signal is proportional to  $\langle \sigma_{(n,n-1)}^{\text{CX}} \rangle$ , the capture cross-section of the charge exchange reaction, and the density of the injected impurity nuclei  $N^Z$ . In this case, the theoretical estimations with small values of both capture-radiation cross-section and NBI density flux in the case of LHD result in two orders of

magnitude smaller CXRe signal value for Li tracer material. This explains why no detectable signal has been observed in LHD TESPEL experiments with LiH tracer before. Therefore, based on the theoretical calculation of the operational range of the TESPEL CXRe diagnostics in the visible spectral range under the conditions of the LHD plasma ( $E_{\text{NBI}} = 150$  keV) [2], the TESPEL CXRS experiments with tracer materials, such as fluorine ( $\lambda_{\text{F}(n=10 \rightarrow 9)} = 479.3$  nm) and magnesium ( $\lambda_{\text{Mg}(n=12 \rightarrow 11)} = 478.9$  nm) have been carried out. From simple estimations the increase of the CXRe signals in these cases up to the signal level that was observed on the CHS machine with LiH tracer is expected.

## 2. Setup of TESPEL CXRS diagnostic on LHD

The basic idea of this method is illustrated in Fig. 1. When injected TESPEL enters into the plasma, the outer layer is ablated first, delivering the tracer core to the inner plasma region. After ionization, the fully stripped tracer ions move along the magnetic field lines forming a toroidal annular X ions domain as shown in Fig. 1, which later diffuses in the radial direction. The long time scale diffusion in the radial direction of the fully ionized impurity ions from this localized domain can be measured by the observation of charge exchange recombination (CXRe) emission intensity due to the

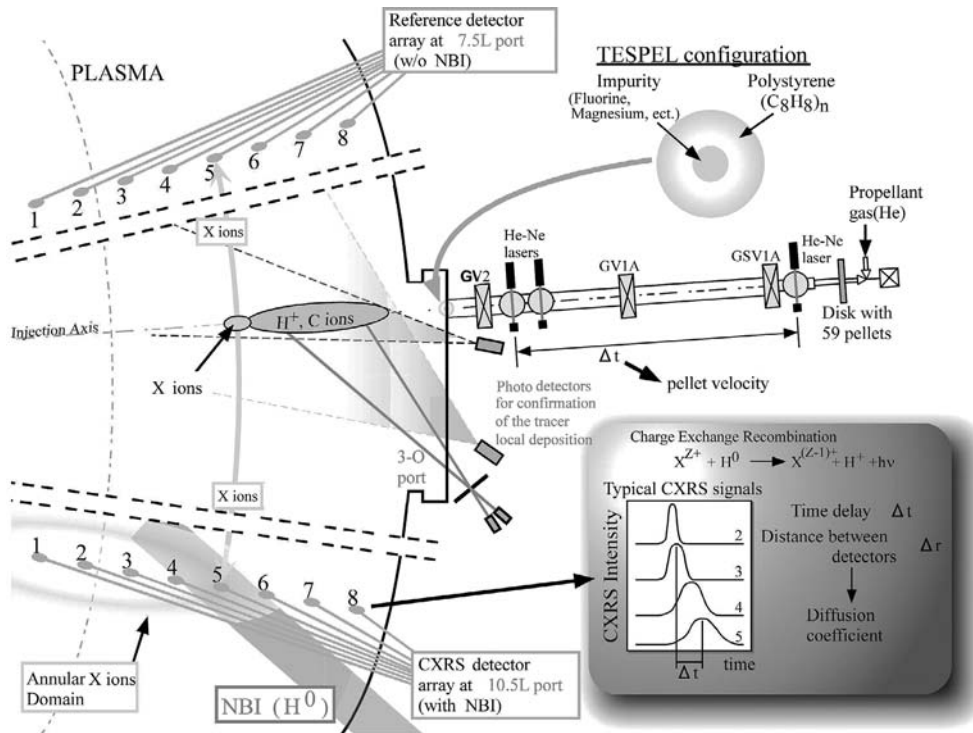


Fig. 1 Schematic view of the TESPEL pellet injection system.

CX reaction of injected impurity nuclei  $I^Z$  (of nuclear charge  $Z$ ) with the neutral beam injection (NBI) hydrogen atoms (assumed to be in their ground state). In our experiments, the CXR signal is measured within a certain visible spectral range. The  $I^{Z-1}$  ions can also exist in the peripheral plasma with low electron temperature due to recombination of  $I^Z$  ions. For this reason, the  $I^Z$  light is observed simultaneously at the location on the NBI path and, for reference, at the neighboring port without the NBI (see in Fig. 1). The light emission from the two arrays of the photo detectors having different radial positions in the NBI port together with the reference detector array in the port without NBI, is transmitted through the optical fibers with 200  $\mu\text{m}$  in diameter to a spectrometer with an Intensified CCD camera. The typical exposure time of this system is 15 ms, therefore the instrument can provide multiple spectra during a plasma discharge with time interval of about 40 ms. The subtraction of the reference signals from the CXR detector signals can be interpreted as pure CXR signals.

### 3. Experimental results in the visible spectral range

The operational limits of the use of TESPEL CXRS diagnostics in the visible spectral range on LHD have been determined which provide a maximum CXR signal assuming that the complete ionization time has to be much smaller than the impurity transport time [2]. Under our experimental conditions (electron temperature  $T_e = 1\text{--}3$  keV and density  $n_e = 0.5\text{--}2 \times 10^{13} \text{ cm}^{-3}$  with NBI power  $P_{NBI} = 3$  MW), there are two types of impurity tracers:

- a Teflon ( $\text{C}_2\text{F}_4$ )<sub>n</sub> block for observing fluorine ( $Z = 9$ )

line at the  $\lambda_{F(n=10 \rightarrow 9)} = 479.3$  nm wavelength

- and magnesium powder for observing magnesium ( $Z = 12$ ) CXR line at  $\lambda_{Mg(n=12 \rightarrow 11)} = 478.9$  nm.

In our experiments, the outer diameter of TESPEL has ranged from 700 to 900  $\mu\text{m}$ . Since it takes much time to evaluate the amount of these impurities due to its amorphous shape, we assumed here that the 50 % ( $\sim 2 \times 10^{-12} \text{ m}^{-3}$ ) by volume of the inner core of the TESPEL is occupied by the tracer material. Then, the total amounts of the impurities injected by TESPEL approximately are  $10^{17}$  for the F tracer, and  $9 \times 10^{16}$  for the Mg tracer, respectively. The expected brightness of the visible CXR light should be about  $1.5 \times 10^{11}$  (ph/cm<sup>2</sup>sr s) and  $10^{11}$  (ph/cm<sup>2</sup>sr s) for Mg and F, respectively. For comparison it is two orders larger than that in the Li impurity case ( $10^9$  (ph/cm<sup>2</sup>sr s)) [4]. In the case of the F tracer, a small signal was observed at one of the eight channels. In the case of the Mg tracer, the CXR emission signal was not observed. As was mentioned before, the CXR signals for the fixed geometry are proportional both to the capture cross-section and to the density of injected impurity nuclei. According to the theoretical calculations the tracer material was chosen as the impurity with the optimal value of the cross-section for LHD plasma conditions, so the possible reason for no detectable signal could be in the small amount of the injected impurity into the LHD plasma. For comparison with the results, the CXR emissions of the other impurities, such as neon ( $\lambda_{Ne(n=11 \rightarrow 10)} = 524.9$  nm), boron ( $\lambda_{B(n=7 \rightarrow 6)} = 494.6$  nm) and carbon ( $\lambda_{C(n=8 \rightarrow 7)} = 529.3$  nm), were investigated. This could be done after the impurity injection, through gas puffing on pure pellet injection. Unfortunately it is difficult to

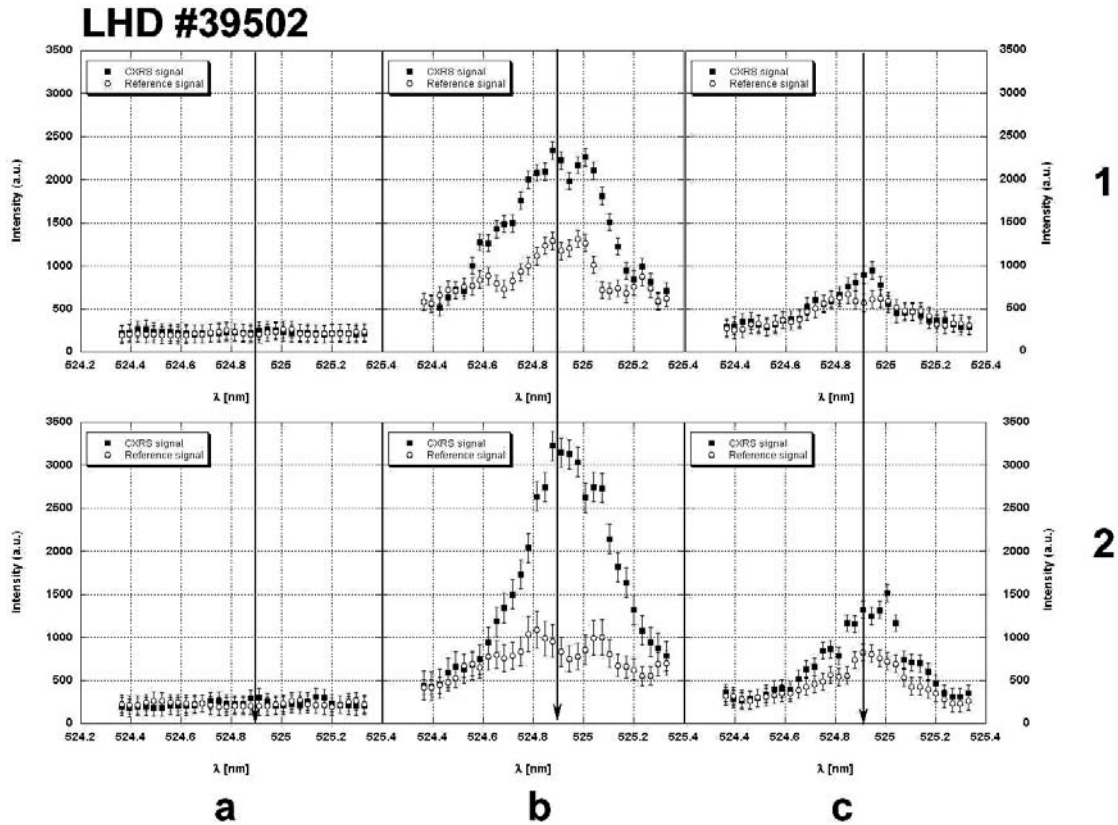


Fig. 2 Ne IV emission at the location of NBI (CXRS) and the reference location for two different channels ( $\rho = 0.9(1)$ ,  $\rho = 0.8(2)$ ) before Ne pellet injection  $t = 0.4$  sec (a), just after  $t = 0.3$  6sec (b) and 350 ms after injection (d).

estimate the impurity amount after the neon gas puff or boronization of the LHD vessel, so we cannot make a comparative analysis of the CXR signals with TESPEL. In the case of the pure impurity pellet, the total amount of the impurity in that is approximately  $3 \times 10^{19}$  and  $1 \times 10^{20}$  for neon and carbon, respectively, which is several orders of magnitude more than in the case F or Mg TESPEL. However, the radiation cross-section for neon ( $11 \times 10^{-18} \text{ cm}^2$ ) under LHD conditions is almost the same as for fluorine ( $9 \times 10^{-18} \text{ cm}^2$ ). Therefore, due to the larger amount of neon impurity, from theoretical estimation the CXR signal should be more than two orders of magnitude larger than was expected for the fluorine case. One example of the signals from detectors with NBI and without NBI just before and after Ne pellet injection for the two different channels is presented in Fig. 2. in the case of the magnetic axis  $R_{ax} = 3.75$  m and magnetic field  $B = 2.6$  T. These two channels are corresponding to the different radial positions indicated by  $\rho$ -values. As shown in Fig. 2a no signals are detectable before pellet injection for both the CXRS and Reference channels cases. At the moment after pellet injection the signals are detectable in the several channels and the maximum appears later for the outer radii (effective radius ( $\rho = 0.9$ ), since a pure pellet begins to ablate from the plasma edge (Fig. 2b). In this case, the relative intensity of the CXR signal measured at the plasma periphery was more than one order of magnitude larger than the F tracer CXR signal level measured, as it was expected from the

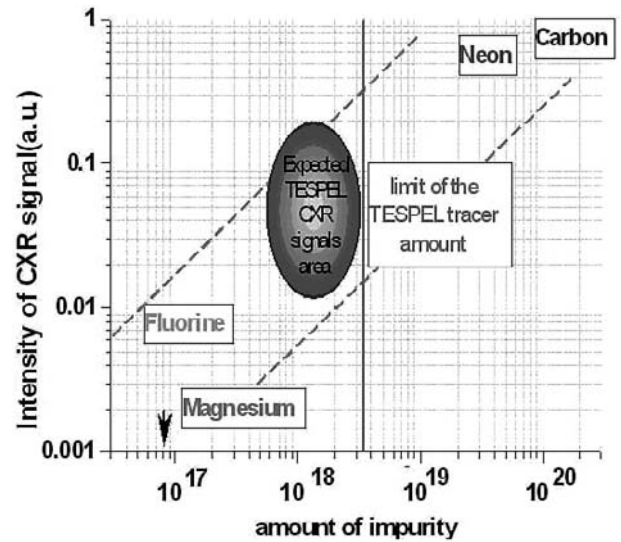


Fig. 3 Comparison of the CXR signal intensity measured in the visible spectral range from the TESPEL (fluorine ( $\lambda_F = 479.3$  nm), magnesium ( $\lambda_{Mg} = 478.9$  nm)) and from the pure impurity pellet (neon ( $\lambda_{Ne} = 524.7$  nm) and carbon ( $\lambda_C = 529$  nm)). The amount of the impurities was different.

theoretical calculations. Based on these experimental results from the CXR emissions of neon and carbon pellets the simple estimation of optimizations of the TESPEL CXRS diagnostics are shown in Fig. 3.

Judging from these experimental results, the CXR signals in the visible range can be increased by several times by increasing the tracer amount up to the TESPEL limit as shown in Fig. 3, if we assume the same level of the coefficient of visible light emission for each tracer material. Theoretically, the inner core volume in the current TESPEL setup can be increased up to  $6 \times 10^{-11} \text{ m}^{-3}$  that is several times more than that we usually used. In this case the resulting tracer amount will be increased up to  $2 \times 10^{18}$ . According to the Fig. 3, the CXRS signal in this case should be increased by several times in comparison with the observed signal from fluorine tracer with a smaller impurity amount ( $10^{17}$ ). The amount of impurity in the recent experiments was increased only up to  $3 \times 10^{17}$  for the fluorine and up to  $8 \times 10^{17}$  for the magnesium case, due to some technical problems to produce a pellet with a limited tracer amount. According to Fig. 3 the CXR signal for fluorine TESPEL should be increased by two times. As for the magnesium TESPEL case with the higher amount of the impurity we cannot extrapolate to a real value, since in the experiments with the smaller magnesium tracer amount the CXRS signals were not detectable. Unfortunately the subtracted CXR signals in the recent experiments are still marginal in some channels, thus we cannot utilize them for transport study on LHD with good quality.

#### 4. Discussion

As an alternative method to obtain larger CXRS signals, it would be preferable to use measurements in the low wavelength region, such as the Ultra Soft X-Ray (USXR) and VUV (Vacuum UltraViolet) spectral ranges [5]. As is well known, for the  $\Delta n = 1$  transitions at shorter wavelengths in the case of small  $n$  the capture radiation cross-section will be increased by several times. From similar theoretical estimations that have been done for the visible spectral range, for the VUV and USXR spectral range the brightness of the CXR signals for the TESPEL case is expected to be about  $4.2 \times 10^{12} \text{ (ph/cm}^2\text{sr s)}$  for F IX line at 8 nm and up to  $10^{13}$  for Mg XII line at 4.5 nm. For the estimations of the applicability of TESPEL CXRS diagnostics in the USXR

range under the usual LHD plasma conditions we took half of the maximum possible tracer amount. The increase by a factor of more than one order of magnitude of the estimated CXRS signal in the USXR spectrum has a clear advantage in comparison to the measurements in the visible spectral range. In the nearest future a new diagnostics system including a high throughput planar multilayer monochromator for the ultrasoft X-ray (USXR) TESPEL CXRS experiments with fluorine and magnesium tracer materials is planned to be installed for the next step.

#### 5. Conclusions

The anticipated increase of the TESPEL CXR signals in the recent experiments, even with limited tracer amounts of magnesium and fluorine was not observed. So we cannot utilize the visible spectral range for transport study on LHD with good quality.

The applicability of the TESPEL CXRS diagnostics in the USXR spectral range in comparison with that in the visible spectral range has been estimated. The increase by a factor of more than one order magnitude in the USXR spectral range has a clear advantage to the TESPEL CXRS diagnostics in the visible spectral range.

#### Acknowledgements

The authors would like to thank members of LHD experimental groups and NIFS personnel for their kind cooperation.

#### References

- [1] K. Khlopenkov and S. Sudo, *Plasma Phys. Control. Fusion* **43**, 1547 (2001).
- [2] V.Yu. Sergeev *et al.*, *Plasma Phys. Control. Fusion* **44**, 277 (2002).
- [3] R.K. Janev, L.P. Presnyakov and V.P. Shevelko, *Physics of Highly Charged Ions* (Berlin: Springer, 1983).
- [4] S. Sudo *et al.*, *Plasma Phys. Control. Fusion* **44**, 129 (2002).
- [5] Isler, *Plasma Phys. Control. Fusion* **36**, 171 (1994).